Dalton Transactions

ROYAL SOCIETY OF CHEMISTRY

PAPER

View Article Online
View Journal

Cite this: DOI: 10.1039/d5dt03086b

Unraveling the structural features of Dion–Jacobson-type layered perovskite-related material $HCa_2Nb_3O_{10}\cdot1.5H_2O$

Zihao Zhang, [a] Jun Kano, *[a] Shu Morita, [b] Hiromu Shimokawa [e] and Minoru Osada [c,d]

Hydrated layered oxides are widely encountered, yet the presence of disordered interlayer water often complicates crystal structure determination from laboratory X-ray diffraction. Here, we report the crystal structure of the Dion–Jacobson-type layered perovskite-related material $HCa_2Nb_3O_{10}\cdot1.5H_2O$, solved from synchrotron X-ray diffraction data by combining direct methods in reciprocal space, Le Bail whole-pattern fitting, and Rietveld refinement. The hydrate crystallizes in a tetragonal structure with space group $P4_22_12$ (a = 7.7070(5) Å, c = 32.4870(3) Å). Incorporation of partially occupied interlayer water-oxygen sites on the (110) plane at z = 0 and 1/2 successfully reproduces the low-angle 00l reflections while preserving the $Ca_2Nb_3O_{10}$ framework. The resulting crystallographic model explicitly resolves the arrangement of interlayer water molecules and provides a robust structural foundation for band-structure calculations as well as for the rational design of hydration-controlled intercalation, exfoliation, and composite materials based on layered perovskite-related materials.

Received 27th December 2025,
Accepted 27th May 2026

DOI: 10.1039/d5dt03086b

rsc.li/dalton

1 Introduction

Layered perovskite-related materials have attracted increasing attention for electronic and energy applications, owing to their structurally tunable frameworks and rich physical properties.[1–4] Among them, Dion–Jacobson (DJ)-type oxides consist of negatively charged perovskite-derived slabs separated by exchangeable interlayer cations, giving rise to pronounced structural anisotropy and exceptional ion-exchange and intercalation capabilities. These features make DJ-type oxides versatile platforms for the construction of composite materials and two-dimensional (2D) nanosheets. Through interlayer ion exchange, intercalation, and exfoliation processes, extensive structural design strategies have been developed, enabling the transformation of bulk layered oxides into 2D nanosheets, thin films, superlattices, and functional hybrid materials.[5] Within this material family, protonated DJ-type oxides such as $HCa_2Nb_3O_{10}$ (HCNO) and their hydrated derivatives have been extensively investigated as photocatalysts for hydrogen evolution from water under ultraviolet irradiation.[6] Previous studies have demonstrated that the photocatalytic activity of HCNO hydrates is highly sensitive to the hydration state and the nature of interlayer species. Interlayer H_2O/H_3O^+ ions are thought to facilitate proton conduction while modulating interlayer spacing and charge-carrier migration through hydrogen-bond networks and electrostatic screening effects, thereby influencing the overall photocatalytic performance.[7] Moreover, hydrated and protonated DJ-type oxides serve as essential precursors for further intercalation of organic amines, incorporation of macromolecular species, and immobilization of metal nanoparticles, with interlayer water playing a critical role in ion-exchange reactions, osmotic swelling, and exfoliation behavior in aqueous media.[5,8] Despite their functional importance, detailed structural information on DJ-type hydrates, including HCNO hydrates, remains scarce. Most previous studies have relied on laboratory X-ray diffraction and thermal analysis to derive average lattice parameters and estimate water content. Consequently, the precise crystallographic locations of interlayer water molecules, their coordination environments, and their spatial relationship with the framework of the perovskite-derived slabs have not been systematically elucidated.[7] This lack of structural insight hampers a fundamental understanding of how hydration governs the physical and chemical pro-

[a]Faculty of Environmental, Life, Natural Science and Technology, Okayama University, Okayama 700-8530, Japan. E-mail: kano-j@cc.okayama-u.ac.jp
[b]Institute of Materials and Systems for Sustainability (IMaSS), Nagoya University, Nagoya 464-8601, Japan
[c]Department of Materials Chemistry and Institute of Materials and Systems for Sustainability (IMaSS), Nagoya University, Nagoya 464-8601, Japan
[d]Research Institute for Quantum and Chemical Innovation, Institutes of Innovation for Future, Society, Nagoya University, Nagoya 464-8601, Japan
[e]Graduate School of Interdisciplinary Science and Engineering in Health Systems, Okayama University, Okayama 700-8530, Japan

perties of DJ-type oxides and limits rational structural design for subsequent intercalation and exfoliation processes. In this study, we focus on the hydrated phase $HCa_2Nb_3O_{10}{\cdot}1.5H_2O$ as a representative DJ-type hydrate, whose hydration stoichiometry was established by thermogravimetric analysis (TGA) in early studies and has been consistently reported in subsequent work.[9] Single-phase samples were synthesized by carefully controlling the proton-exchange and hydration conditions, and their crystal structures were refined using synchrotron X-ray diffraction (SR-XRD). Based on these data, we establish a reliable crystallographic model that explicitly resolves the arrangement of interlayer water molecules and interlayer cations. This structural model provides a robust crystallographic foundation for understanding hydration-induced functionalities in DJ-type oxides and offers a structural basis for future studies on intercalation chemistry, exfoliation into nanosheets, and the design of advanced composite materials.

2 Analytical procedure

The HCNO hydrate ($HCa_2Nb_3O_{10}{\cdot}1.5H_2O$) was obtained by proton exchange of $KCa_2Nb_3O_{10}$ (KCNO) followed by hydration, and the dehydrated (non-hydrated) HCNO phase ($HCa_2Nb_3O_{10}$) was obtained by drying the hydrate. The detailed procedure is described in our previous work.[10] In that study, the crystal structures of the precursor KCNO and the dehydrated (obtained by dry process) HCNO phase were determined by Rietveld refinement of SR-XRD data and were assigned to the monoclinic space group $P2_1/m$ and the tetragonal space group $P4_22_12$, respectively, with complete atomic positional and displacement parameters reported there. In this study, we focus on the hydrated HCNO. SR-XRD patterns were collected with a photon energy of 15.50 keV at Beamline BL5S2, Aichi Synchrotron Radiation Center. Diffraction-pattern indexing and direct methods in reciprocal space for structure solution as a probabilistic space-group search were carried out with EXPO2014, which ranks candidate space groups using normalized-intensity statistics and extinction-symbol analysis.[11] To refine the tetragonal unit-cell parameters and obtain integrated reflection intensities for checking extinction conditions, a Le Bail whole-pattern fit in $P4/mmm$ was performed using the GSAS-II program.[12] These results, together with the EXPO2014 space-group search, provided the basis for subsequent Rietveld refinements using RIETAN-FP.[13]

3 Results and discussion

Fig. 1a shows the SR-XRD pattern of HCNO hydrate. For comparison, the patterns of dehydrated HCNO and KCNO are shown in Fig. 1b and c, respectively. Although our previous study successfully refined the structures of KCNO and dehydrated HCNO by the Rietveld method, all of the patterns are presented here with Le Bail whole-pattern fitting in order to clarify the structural evolution from the parent KCNO phase through protonation and subsequent dehydration. The precursor KCNO was previously determined to adopt the monoclinic space group $P2_1/m$, whereas dehydrated HCNO adopts the tetragonal space group $P4_22_12$.[10] HCNO hydrate can likewise be indexed using a tetragonal cell, which is here described in $P4/mmm$. The diffraction patterns show that all samples show practically a single phase, with all reflections assignable to the layered perovskite phase and no detectable impurity peaks. KCNO, which is the parent material of HCNO, serves as the precursor reference, whereas comparison between dehydrated HCNO and HCNO hydrate clarifies the structural changes associated with hydration. Comparison of the lattice parameters shows that hydration mainly increases the lattice parameter along the stacking direction, with only a minimal change in the in-plane parameter. The elongation of the c-axis upon hydration may reflect not only an expansion of the inter-

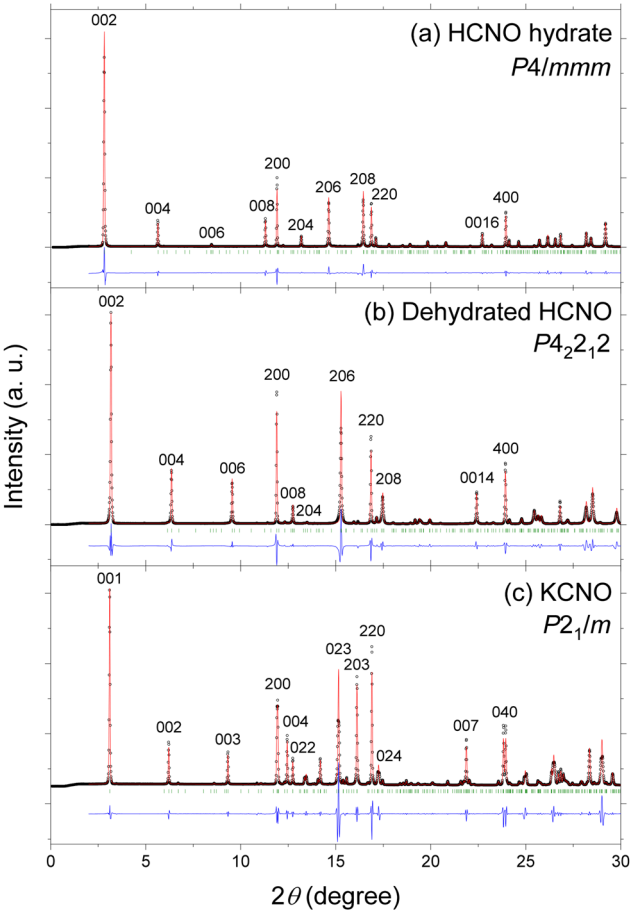

Fig. 1 SR-XRD patterns of (a) HCNO hydrate, (b) dehydrated HCNO, and (c) KCNO. The observed data are presented as open circles, together with the simulated (red lines) and difference (blue lines) patterns obtained by the Le Bail method installed in the GSAS-II program. The vertical green lines indicate the reflection positions. Reflections indexed by the Le Bail method are labeled with *hkl*. The refined lattice parameters are as follows: (a) HCNO hydrate with the tetragonal space group $P4/mmm$, a = 7.7101(11), c = 32.4990(4) Å, R_{wp} = 12.64, and S = 2.23; (b) dehydrated HCNO with $P4_22_12$, a = 7.7133(13), c = 28.7965(5) Å, R_{wp} = 17.40, and S = 2.29; and (c) KCNO with $P2_1/m$, a = 7.7494(2), b = 7.7110(14), c = 14.8832(5) Å, β = 97.442(16)°, R_{wp} = 15.23, and S = 1.64.

layer region but also hydration-related effects on the $Ca_2Nb_3O_{10}$ framework. Thus, the observed increase in the *c*-axis lattice parameter should not be interpreted simply as the geometric size of an inserted water molecule, because the crystallographic *c* parameter also includes the thickness and subtle relaxation of the $Ca_2Nb_3O_{10}$ framework. This interpretation is consistent with the systematic shift of reflections with non-zero *l* indices toward lower 2θ, whereas the *hk*0 reflections remain nearly unchanged. The overall correspondence between the major reflections of HCNO hydrate and dehydrated HCNO suggests that the basic layered framework is largely retained upon hydration, with the principal structural change occurring along the stacking direction. For direct structural comparison with HCNO hydrate, the fractional atomic coordinates and isotropic displacement parameters of dehydrated HCNO are also provided in Table S1 of the SI.

For the assignment of the space group of HCNO hydrate, diffraction pattern indexing and space group candidate searching were performed using EXPO2014 software after peak-shape modelling and background subtraction.[11] The indexing figures of merit indicated that the crystal belongs to the tetragonal crystal system, and the extinction-symbol analysis of the normalized intensities indicated that its Bravais lattice is of primitive (*P*)-type.[14,15] Subsequently, a Le Bail whole-pattern decomposition was performed in the tetragonal space group *P*4/*mmm*, which has no systematic extinctions, to refine the unit-cell metrics and profile parameters. To assess the possible presence of a superstructure, peak positions were compared on the basis of whole-pattern Le Bail fitting using several candidate cells derived from the parent tetragonal lattice. Smaller trial cells, including $a \times a \times c$ and $\sqrt{2}a \times \sqrt{2}a \times \sqrt{2}c$, were also examined, but they failed to reproduce the additional weak reflections. Among the tested models, the $2a \times 2a \times 2c$ supercell provided the best overall match (see Fig. S1, SI). Using this refined cell, the space group determination module of EXPO2014 evaluated candidate extinction symbols based on systematic absences and the statistics of normalized intensities. Among the tetragonal space groups proposed by EXPO2014, $P4_22_12$ and its minimal supergroup $P4_2/nbc$ received the highest scores. Other high-ranking candidates were likewise *P*-type tetragonal space groups with $P4_2$-derived symmetry, which are supergroups of $P4_22_12$ in the group–subgroup hierarchy, reinforcing the above assignment of a *P*-type tetragonal lattice. According to the group–subgroup relations, $P4_22_12$ can be obtained from $P4_2/nbc$ *via* the maximal-subgroup chain $P4_2/nbc \rightarrow P4_222 \rightarrow P4_22_12$ (overall subgroup index 4), indicating a simple symmetry-lowering relationship between the two candidate space groups. To further verify these candidate results, we compared the integrated reflection intensities obtained from a Le Bail fit in *P*4/*mmm* with the systematic-absence conditions for the candidates. No significant intensity above background was detected for 00*l* with *l* odd or for *h*00 with *h* odd, and *hk*0 reflections satisfied $h + k = 2n$. These observations are consistent with the extinction requirements of $P4_2/nbc$ and $P4_22_12$.

Based on the space group candidates obtained by EXPO2014, together with the extinction verification from integrated intensities of a Le Bail whole-pattern decomposition, Rietveld refinement was carried out by using RIETAN-FP for *P*4/*mmm*, $P4_2/nbc$, and $P4_22_12$.[13] A modified split pseudo-Voigt function with a partial profile relaxation was used as the profile function.[16] Structural models for HCNO hydrate were constructed based on the layer-stacking pattern and cation positions previously established for HCNO.[10] In these models, interlayer water species were not modelled at this stage; such NbO_6 octahedral framework-only configuration will hereafter be referred to as "framework-only model". The resulting models, which contained only the NbO_6 octahedral framework, were refined in *P*4/*mmm*, $P4_2/nbc$ and $P4_22_12$ using the same unit-cell and profile parameters. Note that, due to the plate-like particle shape of the HCNO hydrate, preferred orientation had to be considered, even though the SR-XRD measurements were performed while rotating the sample inside the capillary. A partial profile relaxation was applied in the Rietveld refinement, which improved the fit for the reflections in the low-2θ region.

Fig. 2 shows the result of the Rietveld refinement for the *P*4/*mmm*, $P4_2/nbc$, and $P4_22_12$ space groups. The reliability indices show a clear improvement from *P*4/*mmm* to $P4_2/nbc$ and $P4_22_12$, with the lowest R_{wp} and *S* values obtained for $P4_22_12$, indicating that the lower-symmetry models reproduce the observed intensity distribution more accurately under comparable refinement conditions. Clear differences among the three refinements are observed for reflections that are sensitive to distortions of the NbO_6 octahedral framework, including subtle displacements of the Ca cations within the $Ca_2Nb_3O_{10}$ framework. For the low-angle 00*l* reflections, the difference curves reveal larger deviations in *P*4/*mmm* than in $P4_2/nbc$ and $P4_22_12$, with $P4_22_12$ giving the lowest residuals among the three models. A similar tendency is observed for several reflections shown in the low-2θ region, such as 200, 206, and 208, where the calculated intensities for *P*4/*mmm* deviate more strongly from the observed ones than in the refinements using $P4_2/nbc$ or $P4_22_12$. These differences are consistent with symmetry lowering from *P*4/*mmm* to $P4_2/nbc$ and $P4_22_12$, which allows additional distortion modes of the NbO_6 octahedral framework that are incompatible with *P*4/*mmm*. Nevertheless, even in $P4_22_12$ noticeable deviations remain for reflections in the low-2θ region, particularly the 00*l* series, indicating that a model containing only the NbO_6 octahedral framework does not fully account for the observed scattering intensities. Given that HCNO hydrate has the composition $HCa_2Nb_3O_{10}{\cdot}1.5H_2O$, this remaining discrepancy can be derived from a scattering contribution from interlayer water molecules that is not included in the present framework-only model.

To resolve the remaining discrepancies in the framework without interlayer water molecules, further Rietveld refinements were carried out, introducing crystallization water into the interlayer region of the model. Because hydrogen atoms scatter X-rays only very weakly and their coordinates cannot be determined reliably from powder data,[17] only the oxygen atoms of the interlayer water molecules were refined as crystallographic sites in the model, and the associated hydrogen

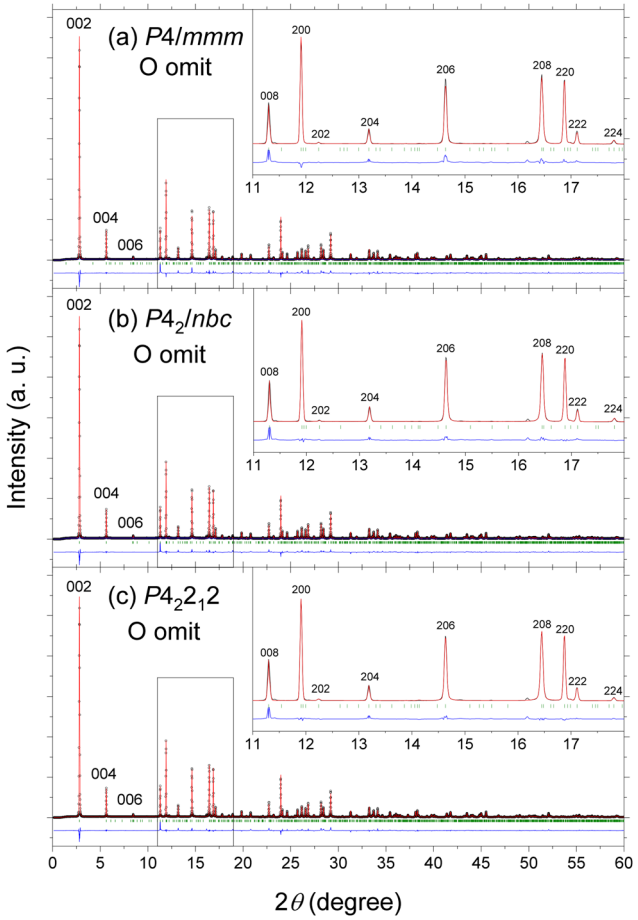

Fig. 2 SR-XRD patterns and fitting results for HCNO hydrate using framework-only models in which interlayer water oxygen atoms were omitted (O omit). The observed data are presented as open circles with simulated (red lines) and difference (blue lines) patterns by the Rietveld refinement. The vertical green lines represent the positions of the reflections. The insets show the reflections located in the low-2θ regions on a magnified scale. Analyzed for (a) *P*4/*mmm*, (b) $P4_2/nbc$, (c) $P4_22_12$. For *P*4/*mmm*, a = 7.7064(8), c = 32.4864(5) Å; R_{wp} = 12.07; and S = 2.15. For $P4_2/nbc$, a = 7.7063(7), c = 32.4869(4) Å; R_{wp} = 10.06; and S = 1.79. For $P4_22_12$, a = 7.7071(7), c = 32.4883(4) Å; R_{wp} = 9.88; and S = 1.76.

atoms were not included in the refinement.[18] In related layered perovskite oxides, distinct hydration arrangements have been reported depending on the interlayer species and the degree of hydration; a bilayer-hydrate model accommodating interlayer K^+ ions solvated by two water layers has been proposed for restacked $KCa_2Nb_3O_{10}\cdot 1.3H_2O$.[19] Such a bilayer arrangement is typically associated with the presence of solvated interlayer alkali cations and may therefore not be directly transferable to the present protonated hydrate. More specific water orientations have also been discussed for stoichiometrically hydrated Ruddlesden–Popper-type oxides, where low-temperature neutron powder diffraction analysis revealed intact H_2O in a vertical "pillared" orientation hydrogen-bonded to apical oxygen atoms.[20] However, because hydrogen atoms are poor X-ray scatterers and their positions are difficult to determine reliably from X-ray powder diffraction data, the present SR-XRD refinement primarily constrains the average positions/occupancies of the interlayer oxygen sites, leaving the H_2O orientation underdetermined. Given the limited sensitivity of X-ray powder data to hydrogen and the likelihood of orientational/disorder effects, we adopted an average-structure description guided by previous neutron-diffraction-based analyses of hydrated layered perovskite oxides, in which interlayer H_2O/H_3O^+ species statistically occupy sites around the body-center of the interlayer cavity defined by apical oxygens of adjacent NbO_6 octahedral layers.[21] Accordingly, the water molecules were assumed to reside around the mid-planes of the interlayer between neighbouring NbO_6 octahedral layers, corresponding to the planes z = 0 and 1/2 in the unit cell. We compared special positions with multiplicities of 2 and 4 against two symmetry-equivalent sets of multiplicity 8 near z = 0 and 1/2, refining a partial occupancy for the latter so that the total interlayer water content matches the nominal stoichiometry of $HCa_2Nb_3O_{10}\cdot 1.5H_2O$; the latter gave lower residuals and was therefore adopted. For schematic visualization of hydrogen bonding, the interlayer H sites were placed at fixed nominal positions slightly displaced from the interlayer water planes, with z = 0.05. Because the present SR-XRD data cannot constrain the precise coordinates of the H sites, these H coordinates were not refined and should not be interpreted as experimentally determined H positions. All other refinement parameters and the NbO_6 octahedral framework model were kept identical to those used in the framework-only refinements described above.

Fig. 3 shows the Rietveld refinement results obtained using models that include partially occupied interlayer water-oxygen sites (O_w) for the *P*4/*mmm*, $P4_2/nbc$ and $P4_22_12$ space groups. Compared with the framework-only refinements in Fig. 2, the agreement factors are further reduced for all three space groups, with $P4_22_12$ again giving the lowest values (R_{wp} = 7.76 and S = 1.38). Hamilton's R-factor ratio test confirms that the improvements obtained with the lower-symmetry models are statistically significant in both the framework-only refinements and the refinements including interlayer water-oxygen sites (Table S2 and Fig. S2, SI).[22] In addition, the difference curves around the low-angle reflections become noticeably flatter for all three models, especially for the 00l series. The deviations around the 002 and 008 peaks that remained in the framework-only model are largely reduced once interlayer water is included in the refinement, and the higher-2θ region also shows smoother difference curves. This indicates that introducing interlayer water improves the overall fit to the diffraction pattern. For $P4_22_12$ in particular, the difference curve is basically flat over the whole 2θ range, apart from a small residual at the intense 002 reflection; no other significant residuals are observed. Although the differences between the three calculated profiles in Fig. 3 are small in appearance, the Rietveld agreement factors still favour $P4_22_12$ over $P4_2/nbc$ and *P*4/*mmm*, in accord with the EXPO2014 space group analysis and with the framework-only refinements in Fig. 2. On this basis, the space group of HCNO hydrate was determined to be $P4_22_12$ as the most appropriate description of HCNO hydrate. Fig. 4,

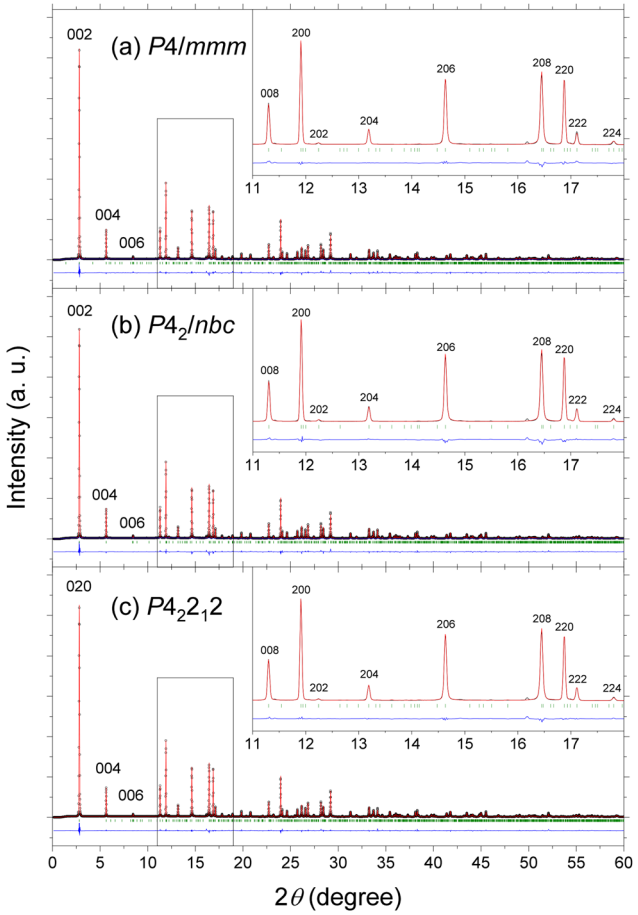

Fig. 3 SR-XRD patterns and fitting results for HCNO hydrate using models including interlayer water-oxygen sites. The observed data are presented as open circles with simulated (red lines) and difference (blue lines) patterns by the Rietveld refinement. The vertical green lines represent the positions of the reflections. The insets show the reflections located in the low-2θ regions on a magnified scale. Analyzed for (a) *P4/mmm*, (b) *P4$_2$/nbc*, (c) *P4$_2$2$_1$2*. For *P4/mmm*, a = 7.7073(6), c = 32.4849 (3) Å; R_{wp} = 9.50; and S = 1.69. For *P4$_2$/nbc*, a = 7.7063(6), c = 32.4846 (3) Å; R_{wp} = 8.46; and S = 1.51. For *P4$_2$2$_1$2*, a = 7.7070(5), c = 32.4870(3) Å; R_{wp} = 7.76; and S = 1.38.

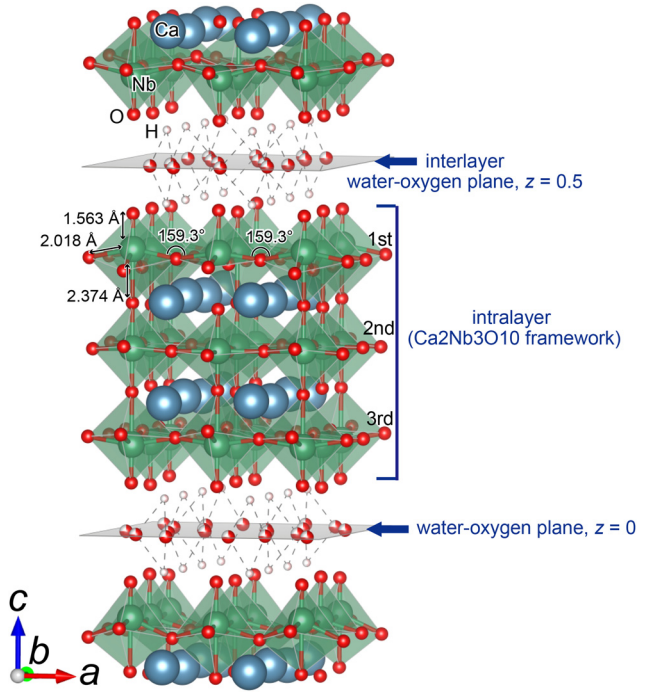

Fig. 4 Layer-stacking model of $HCa_2Nb_3O_{10}\cdot 1.5H_2O$ refined in space group *P4$_2$2$_1$2*, viewed along the *b* axis. Three NbO_6 octahedral layers and the interlayer water-oxygen planes at z = 0 and 1/2 are shown; green octahedra represent NbO_6 units and blue spheres denote Ca atoms, while the white spheres labelled H indicate the protons in HCNO used schematically to illustrate hydrogen bonding. The crystal structures were drawn with VESTA.[23]

drawn using VESTA software,[23] shows the refined crystal structure with the *P4$_2$2$_1$2* space group. The positional disorder of this interlayer water was represented by partially occupied O sites in these planes. The fractional coordinates and isotropic atomic displacement parameters for HCNO hydrate are listed in Table 1, and the unit cell parameters are as follows: a = 7.7070(5) Å, c = 32.4870(3) Å, and Z = 8. Notably, the increase in the *c*-axis lattice parameter is attributed not only to the introduction of intercalated water, which slightly increases the interlayer spacing relative to non-hydrated $HCa_2Nb_3O_{10}$, but also to a subtle influence of the intercalated water on the NbO_6 octahedral framework.

This structural model also raises the question of the appropriate hydration stoichiometry for the refinement. For the refinements including O_w, the hydration stoichiometry of HCNO was also evaluated. Jacobson first reported that HCNO incorporates $1.5H_2O$ upon protonation of KCNO, with the water content determined by TGA.[9] Although many subsequent studies have reported values consistent with this result,[24] larger values (*e.g.*, 1.6 or *ca.* 1.9) have also been reported.[7,25] We therefore examined the sensitivity of the refinement to the occupancy of O_w. Trial refinements in which the O_w occupancy was varied showed only a shallow minimum in R_{wp} as a function of occupancy (Fig. S3, SI), indicating limited sensitivity of the data to this parameter. To maintain consistency and reliability, the O_w occupancy was fixed in the final refinements at the nominal value corresponding to $HCa_2Nb_3O_{10}\cdot 1.5H_2O$, following the nominal composition previously reported by Jacobson.

To further evaluate the local coordination geometry, we examined the bond-valence sums (BVSs) for the refined structure (see Table 1). The relatively high BVS at the Nb2 site (approximately 6.5) is mainly attributable to the presence of two particularly short Nb2–O3 bonds. Because bond valence depends exponentially on bond length, such local shortening can lead to a significant increase in the BVS at a specific site. Therefore, this result should be understood as a local feature of the distorted NbO_6 octahedron rather than as evidence against the overall structural model. This tendency may also be qualitatively consistent with the covalent character of the Nb–O bonds. The resulting structural model is essentially consistent with earlier descriptions of HCNO, and the intercalated

Table 1 The crystallographic data and structural parameters provided by Rietveld analysis. Fractional coordinates and isotropic atomic displacement parameters of HCNO hydrate ($HCa_2Nb_3O_{10}\cdot 1.5H_2O$) with space group $P4_22_12$. Here, g and B denote the site-occupation factor (occupancy) and the atomic displacement parameter of each crystallographic site, respectively. Selected bond valence sum (BVS) values for the framework Nb and O sites are also listed. The BVS values were calculated from the refined bond lengths using the bond-valence expression $V_i = \sum_j \exp\left[(R_0 - R_{ij})/b\right]$, and were evaluated within the $Ca_2Nb_3O_{10}$ framework only

$HCa_2Nb_3O_{10}\cdot 1.5H_2O$ tetragonal $P4_22_12$

a = 7.7070(5) Å, c = 32.4870(3) Å

Atom	Site	g	x	y	z	B (Å^2)	BVS
H1	8g	0.5	1/4	1/4	0.05 (fixed)	0 (fixed)	—
H2	8g	0.5	1/4	3/4	0.05 (fixed)	0 (fixed)	—
Ca1	8g	1	0.2509(16)	0.2535(16)	0.1837(2)	1.31(4)	—
Ca2	8g	1	0.2569(15)	0.7447(17)	0.1790(2)	1.31(—)	—
Nb1	4d	1	1/2	0	0.1151(10)	0.36(3)	5.62
Nb2	4d	1	1/2	0	0.2497(15)	0.36(—)	6.51
Nb3	4d	1	1/2	0	0.3800(12)	0.36(—)	5.20
Nb4	4c	1	0	0	0.1218(15)	0.77(4)	4.70
Nb5	4c	1	0	0	0.2485(19)	0.77(—)	5.26
Nb6	4c	1	0	0	0.3816(15)	0.77(—)	5.25
O_w1	8g	0.75	0.5732(6)	0.2017(5)	0	11.81(105)	—
O_w2	8g	0.75	0.3140(6)	0.1385(5)	0	11.81(—)	—
O1	8g	1	0.2411(6)	−0.0063(7)	0.3641(6)	1.53(12)	2.20
O2	8g	1	−0.0094(6)	0.2436(6)	0.3726(6)	1.53(—)	2.16
O3	8g	1	0.2755(2)	0.0000(4)	0.2451(6)	1.53(—)	2.45
O4	8g	1	−0.0777(14)	0.2532(5)	0.2481(9)	1.53(—)	1.90
O5	8g	1	0.0104(6)	0.2471(5)	0.1300(7)	1.53(—)	2.19
O6	8g	1	0.2553(5)	0.0013(7)	0.1420(6)	1.53(—)	2.01
O7	4d	1	1/2	0	0.0670(13)	5.06(65)	2.56
O8	4d	1	0	1/2	0.0682(15)	5.06(—)	1.84
O9	4d	1	1/2	0	0.3094(13)	5.06(—)	1.78
O10	4d	1	0	1/2	0.3119(14)	5.06(—)	1.57
O11	4c	1	0	0	0.0650(14)	4.40(60)	1.19
O12	4c	1	1/2	1/2	0.0612(12)	4.40(—)	1.15
O13	4c	1	0	0	0.3053(16)	4.40(—)	1.94
O14	4c	1	1/2	1/2	0.3053(16)	4.40(—)	2.26

R_{wp} = 7.76, S = 1.38.

water did not induce any major rearrangement of the $Ca_2Nb_3O_{10}$ framework.

4 Conclusion

In this work, synchrotron powder X-ray diffraction combined with Rietveld analysis establishes $P4_22_12$ as the most appropriate space group for $HCa_2Nb_3O_{10}\cdot 1.5H_2O$. Introducing statistically distributed interlayer water-oxygen sites is essential to reproduce the low-angle 00l intensities, while the $Ca_2Nb_3O_{10}$ framework remains essentially unchanged relative to the dried HCNO phase. Our crystallographic model will contribute toward a reliable basis for subsequent electronic-structure calculations and related theoretical studies.

Author contributions

J. K. proposed the idea, and J. K. and Z. Z. supervised the entire project. S. M. and M. O. provided the synthesis procedure and technical support for sample preparation. Z. Z., S. M., and M. O. prepared the samples. J. K. performed the synchrotron powder X-ray diffraction measurements. Z. Z. carried out the diffraction analysis, including indexing, space-group determination, and Le Bail/Rietveld refinements, under the guidance of J. K. H. S. and Z. Z. evaluated the statistical significance of the refinements using Hamilton's R-factor ratio test. Z. Z. and J. K. interpreted the results. All the authors discussed the results of the study. Z. Z., J. K., S. M., and M. O. co-wrote the manuscript.

Conflicts of interest

The authors declare no competing interests.

Data availability

Crystallographic data for dehydrated HCNO (HCa2Nb3O10) and hydrated HCNO (HCa2Nb3O10·1.5H2O) have been deposited under deposition numbers 2504732 and 2556680, respectively, *via* the CCDC/FIZ Karlsruhe deposition service. Other data supporting the findings of this study are available from the corresponding author upon reasonable request.

Supplementary information (SI) is available. The Supplementary Information includes crystallographic parameters

for dehydrated HCNO (Table S1), comparison of candidate supercells by Le Bail analysis (Fig. S1), statistical evaluation of the Rietveld refinements by Hamilton's R-factor ratio test (Table S2 and Fig. S2), and the Rwp dependence on the constrained Ow occupancy (Fig. S3). See DOI: https://doi.org/10.1039/d5dt03086b.

CCDC 2504732 ($HCa_2Nb_3O_{10}$) and 2556680 ($HCa_2Nb_3O_{10}\cdot 1.5H_2O$) contain the supplementary crystallographic data for this paper.[26a,b]

Additional information, such as input files for calculations and scripts used for analysis, can be provided upon request.

Acknowledgements

We thank Dr Tomohiro Ikeda (Honda R&D Co., Ltd) and Dr Yuuki Nakanishi (Aichi Synchrotron Radiation Center) for technical assistance with the SR-XRD. This work was supported by the JSPS KAKENHI (Grant No. 20KK0330, 20H02609, 21H05015, 22K18976, 24K08247, and 25K22296) and JSPS Program for Forming Japan's Peak Research Universities (J-PEAKS, Grant No. JPJS00420230010).

References

1 M. Osada and T. Sasaki, *Dalton Trans.*, 2018, **47**, 2841–2851.
2 B.-W. Li, M. Osada, Y.-H. Kim, Y. Ebina, K. Akatsuka and T. Sasaki, *J. Am. Chem. Soc.*, 2017, **139**, 10868–10874.
3 H.-J. Kim, S. Morita, K.-N. Byun, Y. Shi, T. Taniguchi, E. Yamamoto, M. Kobayashi, Y. Ebina, T. Sasaki and M. Osada, *Nano Lett.*, 2023, **23**, 3788–3795.
4 S. Morita, D. Urushihara, K. Nishibashi, M. Kobayashi, E. Yamamoto, T. Asaka, H. Nakajima, S. Mori and M. Osada, *J. Am. Chem. Soc.*, 2024, **146**, 25221–25231.
5 R. Uppuluri, A. S. Gupta, A. S. Rosas and T. E. Mallouk, *Chem. Soc. Rev.*, 2018, **47**, 2401–2430.
6 S. Tasleem and M. Tahir, *Int. J. Hydrogen Energy*, 2020, **45**, 19078–19111.
7 M. G. Shelyapina, O. I. Silyukov, E. A. Andronova, D. Y. Nefedov, A. O. Antonenko, A. Missyul, S. A. Kurnosenko and I. A. Zvereva, *Molecules*, 2021, **26**, 5943.
8 T. Sasaki and M. Watanabe, *J. Am. Chem. Soc.*, 1998, **120**, 4682–4689.
9 A. J. Jacobson, J. T. Lewandowski and J. W. Johnson, *J. Less-Common Met.*, 1986, **116**, 137–146.
10 Z. Zhang, N. Oshime, Y. Hamasaki, M. Osada, S. Morita, Y. Takaguchi, M. Yamagami, T. Okubo, K. Horigane, N. Ikeda, T. Fujii, P. Gemeiner, P.-E. Janolin, S. Hirose and J. Kano, *J. Appl. Phys.*, 2026, **139**, DOI: 10.1063/5.0321518.
11 A. Altomare, C. Cuocci, C. Giacovazzo, A. Moliterni, R. Rizzi, N. Corriero and A. Falcicchio, *J. Appl. Crystallogr.*, 2013, **46**, 1231–1235.
12 B. H. Toby and R. B. V. Dreele, *J. Appl. Crystallogr.*, 2013, **46**, 544–549.
13 F. Izumi and K. Momma, *Solid State Phenom.*, 2007, **130**, 15–20.
14 A. Altomare, R. Caliandro, M. Camalli, C. Cuocci, C. Giacovazzo, A. G. G. Moliterni and R. Rizzi, *J. Appl. Crystallogr.*, 2004, **37**, 1025–1028.
15 L. Palatinus and A. van der Lee, *J. Appl. Crystallogr.*, 2008, **41**, 975–984.
16 F. Izumi, *J. Ceram. Soc. Jpn.*, 2003, **111**, 617–623.
17 M. Woińska, S. Grabowsky, P. M. Dominiak, K. Woźniak and D. Jayatilaka, *Sci. Adv.*, 2016, **2**, e1600192.
18 K. A. Selevich, L. S. Ivashkevich, A. F. Selevich and A. S. Lyakhov, *Russ. J. Inorg. Chem.*, 2002, **47**, 1533–1536.
19 Y. Chen, X. Zhao, H. Ma, S. Ma, G. Huang, Y. Makita, X. Bai and X. Yang, *J. Solid State Chem.*, 2008, **181**, 1684–1694.
20 S. Liu, M. Avdeev, Y. Liu, M. R. Johnson and C. D. Ling, *Inorg. Chem.*, 2016, **55**, 1403–1411.
21 S. Nishimoto, M. Matsuda, S. Harjo, A. Hoshikawa, T. Ishigaki, T. Kamiyama and M. Miyake, *J. Solid State Chem.*, 2006, **179**, 3308–3313.
22 W. C. Hamilton, *Acta Crystallogr.*, 1965, **18**, 502–510.
23 K. Momma and F. Izumi, *J. Appl. Crystallogr.*, 2011, **44**, 1272–1276.
24 V. V. Voytovich, S. A. Kurnosenko, O. I. Silyukov, I. A. Rodionov, I. A. Minich and I. A. Zvereva, *Front. Chem.*, 2020, **8**, 300.
25 S. L. Guertin, E. A. Joseph, D. Montasserasadi and J. B. Wiley, *J. Alloys Compd.*, 2015, **647**, 370–374.
26 (*a*) CCDC 2504732: Experimental Crystal Structure Determination, 2026, DOI: 10.25505/fiz.icsd.cc2q2ct0; (*b*) CCDC 2556680: Experimental Crystal Structure Determination, 2026, DOI: 10.25505/fiz.icsd.cc2rtfkl.